Outer Retinal Alterations Associated With Visual Outcomes in Best Vitelliform Macular Dystrophy

Edouard Augstburger, Raphaëlle Orès, Saddek Mohand-Said, Sarah Mrejen, Chafik Keilani, Aline Antonio, Christel Condroyer, Camille Andrieu, José-Alain Sahel, Christina Zeitz, et al.

Outer retinal alterations associated with visual outcomes in Best vitelliform macular dystrophy

Edouard Augstburger[1], Raphaëlle Orès[1], Saddek Mohand-Said[1,2], Sarah Mrejen[1], Chafik Keilani[1], Aline Antonio[2], Christel Condroyer[2], Camille Andrieu[1], José-Alain Sahel[1,2,3], Christina Zeitz[2], Isabelle Audo[1,2]

[1]Centre Hospitalier National d'Ophtalmologie des Quinze-Vingts, Centre de Maladies Rares "dystrophies rétiniennes d'origine génétique", DHU Sight Restore INSERM-DHOS CIC 1423, Paris F-75012, France.

[2]Sorbonne Université, INSERM, CNRS, Institut de la Vision, 17 rue Moreau, F-75012 Paris, France.
[3]Department of Ophthalmology, The University of Pittsburgh School of Medicine, Pittsburgh, PA 15213, United States of America.

Corresponding authors:

Isabelle Audo

Edouard Augstburger

Institut de la Vision

Department of genetics

17, rue Moreau

75012 Paris

France

Telephone: +33 1 53 46 25 42

Email: isabelle.audo@inserm.fr

edouard.augst@gmail.com

Short title: Outer nuclear layer thickness in Best vitelliform dystrophy

Keywords: Best vitelliform macular dystrophy; *BEST1*; structure/function correlation; spectral-domain Optical coherence tomography; outer nuclear layer thickness; Photoreceptor outer segment length.

Introduction

Best vitelliform macular dystrophy (BVMD) is a dominantly inherited macular degeneration with a variable penetrance and expressivity. The classic form of the disease appears during the first two decades of life[(1)], and gradually leads to a loss of

central vision. It was the first form of degeneration that was associated with mutations in *BEST1*, which is located on chromosome 11q12-q13[2-4]. Subsequently, four other clinical entities have been associated with this gene[2,5], and more than 200 mutations[4] have been reported and related to "bestrophinopathies". Bestrophin-1 is the protein encoded by this gene. This integral membrane protein is localized at the basolateral plasma membrane of retinal pigment epithelium (RPE) cells[3,4], is involved in the control of intracellular Ca^{2+} signaling and functions as a Ca^{2+}-activated anion channel[3,6]. This role helps explain the functional abnormalities recorded with the electrooculogram in bestrophinopathies, which manifests as an alteration in the light peak-to-dark trough Arden ratio[5].

The precise origin of the vitelliform material (VM) remains incompletely understood, but some histopathological findings[7,8] and animal models[9,10] have suggested that this material consists of an accumulation of lipofuscin and unphagocytosed photoreceptor outer segments[4,10,11]. The clinical course of the disease is well defined by a progressive accumulation of yellowish VM that splits up and then disappears, as described initially by the Gass classification[12]. For decades, follow-up was limited to the clinical observation of a fundus lesion. The visual field defect is well correlated with the size of the lesion seen on the fundus[13]. However, there are wide variations in visual acuity even with lesions belonging to the same clinical stage[14]. With the first optical coherence tomography (OCT) images, the contents of vitelliform lesions and the dynamics of material accumulation and resorption could be analyzed *in vivo*[15]. However, only the advent of the high-definition spectral domain (SD) OCT[16] allowed the detection of specific alterations of the outer retina[17-21]. It was subsequently highlighted that neither the size of the lesion, nor the amount of VM or subretinal fluid (SRF) had any real impact on visual acuity, unlike the disruption of the ellipsoid zone (EZ)[19], which reflected the specific alteration of photoreceptors[22] at the inner segment / outer segment (OS) interface. However, this interruption is a phenomenon mostly observed in advanced stages of the disease when vision is already severely impaired[16,19]. Moreover, EZ disruption is difficult to quantify, and its analysis during SD-OCT monitoring can be altered by the presence of SRF or hyper-reflective VM. Recently, Duncker et al.[18] identified some differences in the thickness of the outer nuclear layer (ONL) and OS in BVMD patients compared to healthy subjects. The ONL essentially contains the photoreceptor bodies, and its thinning may reflect photoreceptor degeneration, as suggested in other retinal diseases[23-25]. Bestrophinopathies are the most common RPE-related diseases with no current curative treatments. The advances made in recent years in translational research[26] require prompt identification of clinical outcomes for disease progression and prognosis that may be suitable for therapeutic trials.

The purpose of this study was to investigate the SD-OCT morphological impairments of the foveal outer retina in a large cohort of BVMD patients and correlate other SD-OCT markers with visual acuity. The progression of the vitelliform lesion and the occurrence of complications during follow-up were also evaluated using multimodal imaging.

Patients and Methods

Patients

This retrospective cross-sectional study was conducted at the National reference center for rare diseases of the Quinze–Vingts National Ophthalmology Hospital (Paris, France) between February 2011 and November 2018. The clinical charts of BVMD patients with clinically visible lesions and confirmed *BEST1* mutations were reviewed. This study was approved by the local ethics committee and adhered to the principles outlined in the Declaration of Helsinki; written informed consent was obtained from each subject prior to genetic testing (CPP, Comité de Protection des Personnes Ile de France V, project number 06693, N° EUDRACT 2006-A00347-44).

The clinical diagnosis was based on fundus examination, family history and an abnormal Arden ratio on the electrooculogram, later confirmed by genetic testing. BVMD subjects underwent a complete ophthalmologic examination, including an assessment of the best corrected visual acuity (BCVA) according to the standardized Early Treatment Diabetic Retinopathy Study (ETDRS) chart, slit-lamp anterior segment examination, tonometry and fundus examination. SD-OCT and short-wavelength fundus autofluorescence were also performed at each visit. Staging was based on the Gass clinical evolutive classification[12]—stage 1: subclinical with no vitelliform alteration, stage 2: vitelliform, stage 3: pseudohypopyon, stage 4: vitelliruptive and stage 5: atrophic/cicatricial (Figure 1). To avoid biases related to correlations between the two eyes, only the right eyes were included in the analysis. Age-matched control subjects were recruited from hospital workers and patients who consulted in the emergency department. The right eyes were included as a control group (NC group). Exclusion criteria for BVMD and NC subjects were the presence of an associated retinal or choroidal disorder, history of glaucoma, optic neuropathy, uveitis or a significant systemic disorder that may have an impact on ophthalmic assessment.

Spectral-domain OCT data acquisition and processing

High-resolution horizontal SD-OCT cross-sectional B-scans of the macula (25 lines spaced 240 µm apart) were obtained using a Spectralis Heidelberg imaging platform (Spectralis® OCT, Heidelberg Engineering, Dossenheim, Germany). Thirty frames were averaged for each B-Scan. Automatic segmentation with manual adjustment was employed by investigators for recognition of the different retinal layers using Heidelberg Eye Explorer (version 1.7.1.0; Heidelberg Engineering) in accordance with the international reference anatomy[27]. The central subfield thickness (CST) was determined automatically within a 1 mm diameter circle centered on the fovea. Determination of the foveal ONL thickness was done manually perpendicular to the RPE using the "caliper tool" that was included with the Heidelberg analysis software[28] (Heidelberg Engineering, Heidelberg, Germany) (Figure 2). The presence of SRF and VM were determined after analysis of all macular B-scans. Foveal disruptions of the external limiting membrane (ELM) and ellipsoid zone (EZ) were evaluated from the horizontal foveal scan. Due to the resolution of the current SD-OCT images, it was not possible to perform a reliable and discriminating measurement of the length of the photoreceptor outer segment length (PROSL) in the absence of subretinal fluid. For all eyes with SRF, the PROSL was measured from the EZ to the tip of the OS in the horizontal section passing through the fovea. The value selected was an average of three orthogonal measurements of the apical projection of the photoreceptor OS within the subretinal detachment (SRD) in the center of the fovea and 500 µm on either side (Figure 2). Measurements for ONL thickness and PROSL were performed separately and blindly by two of the

investigators, then an average of the measurements was performed for each eye. For eyes that had follow-up assessment of at least one year, the comparative data were those of the initial and last recorded visits.

BEST1 Mutation Analysis

Samples included in this study originate from NeuroSensCol (PI: JA Sahel, coPI: I Audo, partner with CHNO (Centre Hospitalier National d'Ophtalmologie) des Quinze-Vingts, Inserm and CNRS (Centre National de la Recherche Scientifique)). DNA was extracted from peripheral blood samples according to manufacturer recommendations (Puregen Kit, Qiagen, Courtabœuf, France), and all eleven *BEST1* exons were amplified and sequenced for disease-causing mutations (NCBI Reference Sequence: NM_004183.3, primer sequences available upon request). Nucleotide numbering reflects cDNA numbering with +1 corresponding to the A of the ATG translation initiation codon in the reference sequence.

Statistical analyses

All data are presented as median (range). BCVA was converted to the logarithm of the minimal angle of resolution (logMAR) for statistical analyses. Correlations were tested using the Spearman rank correlation coefficient. The Mann-Whitney bilateral test was used to compare data from the BVMD group to the control group. The Wilcoxon rank-sum test was used to compare the differences between baseline and last-visit parameters. The intraclass correlation coefficient (ICC) was used to assess inter-observer reliability. *P*-values < 0.01 were considered statistically significant. XLSTAT 2018 software was used for statistical analyses.

Results

Forty-two eyes from 42 subjects were included in the BVMD group, and 42 eyes from 42 subjects were included in the NC group. All BVMD patients included in this study were heterozygous for a mutation in *BEST1*, in keeping with the autosomal dominant inheritance of the disease. Mutation details for each patient are presented in supplementary table 1. Twenty-six distinct variants were identified in the entire cohort which were all missense changes. Among these variants, 5 were recurrent in apparently unrelated families (i.e. c.47C>T, p.(Ser16Phe) found in 2 families; c.653G>A, p.(Arg218His) found in 4 families; c.692G>C, p.(Ser231Thr) found in 2 families; c.874G>A, p.(Glu292Lys) found in 3 families and c.920C>A, p.(Thr307Asn) found in 2 families). Our genetic screening also identified 7 novel changes with strong pathogenic prediction spanning the entire gene which expand further the mutation spectrum of *BEST1* (see supplementary table 1): c.82A>C, p.(Ile28Leu) on exon 2; c.215A>T, p.(Tyr72Phe) on exon 3; c.294G>C, p.(Glu98Asp) and c.419T>C, p.(Leu140Pro) on exon 4; c.853G>A, p.(Val285Ile) on exon 7; c.924C>A, p.(Asn308Lys) and c.1397G>C, p.(Ser466Thr). These variants co-segregated with the phenotype when additional family members were available.

The overall demographic and OCT characteristics are summarized in Tables 1 and 2. Within the cohort, 43% of patients were male, and the median age was 43.5 (71) years. The distribution according to stage was 4.8% for stage 1, 23.8% for stage 2, 16.6% for stage 3, 45.2% for stage 4 and 9.5% for stage 5. The median BCVA logMAR was 0.40 (2.204) in the BVMD group and 0 (0.25) in the NC group.

SD-OCT characteristics

The median CST was 298 (724) µm, with no significant difference between the experimental and control groups ($P = 0.38$) (Table 2). CST was higher in stage 2, with a value of 416 (724) µm due to the presence of SRF (Table 2). The presence of SRF and VM was noted in 76% and 79% of the BVMD eyes examined, respectively. ICC were 0.97 and 0.94 for ONL thickness and PROSL measurements, respectively. The median ONL thickness was 42 (124 µm) and significantly thinner compared to the control group ($P < 0.0001$). ONL thickness also decreased with stage progression (Table 2). Among patients with SRF, the PROSL was significantly lower as the stage progressed (Table 2). Regarding the ELM and the EZ, foveal disruption was found in 62% and 83% of the BVMD eyes, respectively, these alterations increasing in advanced disease (Table 2).

Correlation

BCVA was correlated with stages ($R = 0.710$; $P < 0.01$), age of patients ($R = 0.448$; $P < 0.01$), and CMT ($R = -0.411$; $P < 0.01$) (Table 3). Regarding the SD-OCT outer retinal alterations, there was a large correlation between BCVA and ONL thickness ($R = -0.620$; $P < 0.01$). Patients with disrupted EZ and ELM had significantly decreased visual acuity compared to others ($P < 0.001$ for both). There was no difference in BCVA between patients with SRD or VM and others ($P = 0.758$ and P = 0.968, respectively). Interestingly, among the 32 eyes with SRD, PROSL was correlated with BCVA ($R = -0.467$; $P < 0.01$) and ONL thickness ($R = 0.444$; $P < 0.01$).

Follow up

Twenty-one eyes from 21 patients had a follow-up visit, with a median of 49 (72) months. Table 4 summarizes all of the characteristics of the eyes that were monitored. Five eyes progressed by one stage, and two eyes progressed by two stages. Fifteen eyes showed a persistent chronic SRD between the initial and last visit. A choroidal neovascularization was noted in one eye and received an appropriate anti-VEGF therapy[29]. There were significant correlations between the initial and final examinations of -0.19 logMAR concerning the BCVA ($P = 0.003$) and -9.2 µm concerning the ONL thickness ($P < 0.001$). The differences for the CST ($P = 0.340$) and PROSL ($P = 0.920$) were not significant (Table 4).

Discussion

In comparison with fundus examination, SD-OCT is a fast and reproducible way of monitoring changes of the different retinal layers in BVMD[15,17–20]. Several recent articles have shown that disruption of the ellipsoid zone during follow-up was the most relevant factor associated with visual acuity loss[19,30]. This phenomenon reflects the direct alteration of photoreceptors through a disruption between their inner and outer segments. These SD-OCT observations were confirmed by adaptive optics scanning laser ophthalmoscopy findings[17,22], where rarefaction of the cones and morphological changes were directly observed within the vitelliform lesion. However, the interruption of the ellipsoidal zone is a phenomenon mainly found in later stages and is associated with already severe visual impairment. Moreover, this anomaly is difficult to quantify, and its visibility during SD-OCT monitoring can be altered by the presence of SRF or hyper-reflective VM.

Our results, from this large cohort of molecularly diagnosed BVMD subjects, indicate that regardless of the clinical stage, ONL thickness measured by SD-OCT was significantly lower in BVMD patients compared to control subjects (Table 2) and was well correlated with BCVA (Table 3 and Figure 3). Despite a short follow-up, measurement of foveolar ONL thickness was found to be a relevant quantitative criterion for documenting an anatomical difference concomitantly with a decreased visual acuity (Table 4). The ONL is essentially composed of the photoreceptor nuclei, which explains the consistent relationship between photoreceptor loss and thinning of the ONL measured in SD-OCT, as initially observed by Mullins et al. in histological samples[7].

The explanation for photoreceptor alteration, while BVMD initially affects RPE, could be related to the presence of chronic SRF secondary to the altered adhesion within the RPE–photoreceptor complex. With an interesting SD-OCT analysis, Qian et al. suggested that thinning and degeneration of RPE is the main reason for chronic SRF, and it occurs by altering the pump function located at the apical side of the RPE cells[30]. In the long term, the accumulation of SRF leads to a loss of cell-to-cell contact between the photoreceptors and the RPE, causing a loss of OS by lack of renewal and, thus, apoptosis of the foveolar cone cells[7,31]. Singh et al. also suggested that *BEST1* mutations lead to reduced clearance of photoreceptor OS and might predispose RPE to enhanced oxidative stress[11].

Many patients with SRF present with a good preservation in visual acuity, even after several years of evolution. In fact, we can observe an elongation of the OS of the photoreceptors in the early phase, which are normally phagocytosed by the RPE with which they are no longer in contact. However, with the persistence of the SRF, we observe a shortening of the OS, which gradually disintegrates and then disappears before being replaced by atrophy (Figure 1). This is in agreement with the fact that the PROSL decreases with the progression of stages (Table 2).Thus, during follow-up, a progressive decrease in BCVA is observed due to the disappearance of the foveolar cones, leading to a progressive thinning of the foveal ONL[32]. Unfortunately, we probably did not have a sufficient number of patients with SRD or a long enough follow-up to successfully demonstrate a significant difference in PROSL.

Although in central serous chorioretinopathy (CSC) the RPE anomaly and the mechanism responsible for the SRD is different, Matsumoto et al. reported similar observations regarding photoreceptor degeneration within the SRD. Comparing eyes affected with CSC to control subjects, they highlighted the presence of elongated protruding OS inside the SRD due to an incomplete phagocytic cycle by RPE[33]. Similarly to our observations in BVMD patients, chronic SRF in CSC leads to an impairment of photoreceptors and ONL thinning[24,34], which is also correlated with BCVA[25,32].

The measurement of only one horizontal scan passing through the fovea can cause a bias, as the measured parameters may vary from one scan to another. However, the slice was generated automatically, with manual adjustment in controversial cases and the same section was performed for all eyes from one visit to the next using the tracking system. Similarly, the ONL measurement at the foveolar level has a confounding factor related to the presence of the Henle fiber layer (HFL).

Nevertheless, the fovea is in the retinal zone where HFL is the thinnest and where the ONL measurement is the most reproducible[35].

Our results demonstrate that, regardless of stages, the thickness of foveolar ONL and PROSL (within the SRD) are correlated with visual acuity (Table 3 and Figure 3) and are a simple way to indirectly monitor photoreceptor alterations and disease progression in BVMD patients. In the future, these parameters could be used to monitor the effects of therapeutic approaches[36].

References

1. Blodi CF, Stone EM. Best's vitelliform dystrophy. *Ophthalmic Paediatr Genet.* 1990;11(1):49–59.

2. Boon CJF, Klevering BJ, Leroy BP, Hoyng CB, Keunen JEE, den Hollander AI. The spectrum of ocular phenotypes caused by mutations in the BEST1 gene. *Progress in Retinal and Eye Research.* 2009;28(3):187–205.

3. Marmorstein AD, Marmorstein LY, Rayborn M, Wang X, Hollyfield JG, Petrukhin K. Bestrophin, the product of the Best vitelliform macular dystrophy gene (VMD2), localizes to the basolateral plasma membrane of the retinal pigment epithelium. *Proc Natl Acad Sci USA.* 2000;97(23):12758–63.

4. Johnson AA, Guziewicz KE, Lee CJ, et al. Bestrophin 1 and retinal disease. *Prog Retin Eye Res.* 2017;58:45–69.

5. Marmorstein AD, Cross HE, Peachey NS. Functional roles of bestrophins in ocular epithelia. *Prog Retin Eye Res.* 2009;28(3):206–26.

6. Sun H, Tsunenari T, Yau K-W, Nathans J. The vitelliform macular dystrophy protein defines a new family of chloride channels. *Proc Natl Acad Sci USA.* 2002;99(6):4008–13.

7. Mullins RF, Oh KT, Heffron E, Hageman GS, Stone EM. Late development of vitelliform lesions and flecks in a patient with best disease: clinicopathologic correlation. *Arch Ophthalmol.* 2005;123(11):1588–94.

8. Zhang Q, Small KW, Grossniklaus HE. Clinicopathologic findings in Best vitelliform macular dystrophy. *Graefe's Archive for Clinical and Experimental Ophthalmology.* 2011;249(5):745–51.

9. Zhang Y, Stanton JB, Wu J, et al. Suppression of Ca2+ signaling in a mouse model of Best disease. *Hum Mol Genet.* 2010;19(6):1108–18.

10. Guziewicz KE, Sinha D, Gómez NM, et al. Bestrophinopathy: An RPE-photoreceptor interface disease. *Progress in Retinal and Eye Research*. 2017;58:70–88.

11. Singh R, Shen W, Kuai D, Martin JM, et al. iPS cell modeling of Best disease: insights into the pathophysiology of an inherited macular degeneration. *Human Molecular Genetics.* 2013; 22(3):593–607.

12. Gass JDM. Stereoscopic atlas of macular diseases: diagnosis and treatment. 3rd ed. St Louis. Mosby; 1987. 502 p.

13. Querques G, Atmani K, Bouzitou-Mfoumou R, Leveziel N, Massamba N, Souied EH. Preferential hyperacuity perimeter in best vitelliform macular dystrophy. *Retina.* 2011;31(5):959–966.

14. Fishman GA, Baca W, Alexander KR, Derlacki DJ, Glenn AM, Viana M. Visual acuity in patients with best vitelliform macular dystrophy. *Ophthalmology.* 1993;100(11):1665–70.

15. Spaide RF, Noble K, Morgan A, Freund KB. Vitelliform Macular Dystrophy. *Ophthalmology.* 2006;113(8):1392-1400.

16. Querques G, Regenbogen M, Quijano C, Delphin N, Soubrane G, Souied EH. High-Definition Optical Coherence Tomography Features in Vitelliform Macular Dystrophy. *American Journal of Ophthalmology.* 2008;146(4):501-507.

17. Kay DB, Land ME, Cooper RF, et al. Outer Retinal Structure in Best Vitelliform Macular Dystrophy. *JAMA Ophthalmology.* 2013; 131(9):1207.

18. Duncker T, Greenberg JP, Ramachandran R, et al. Quantitative Fundus Autofluorescence and Optical Coherence Tomography in Best Vitelliform Macular Dystrophy. *Investigative Opthalmology & Visual Science.* 2014; 55(3):1471.

19. Querques G, Zerbib J, Georges A, et al. Multimodal analysis of the progression of Best vitelliform macular dystrophy. *Mol Vis.* 2014; 20:575–92.

20. Battaglia Parodi M, Iacono P, Romano F, Bandello F. SPECTRAL DOMAIN OPTICAL COHERENCE TOMOGRAPHY FEATURES IN DIFFERENT STAGES OF BEST VITELLIFORM MACULAR DYSTROPHY. *Retina* 2018;38(5): 1041-1046.

21. Parodi MB, Romano F, Sacconi R, et al. INTRARETINAL HYPERREFLECTIVE FOCI IN BEST VITELLIFORM MACULAR DYSTROPHY. *Retina* 2018;38(12) :2379–86.

22. Scoles D, Sulai YN, Cooper RF, et al. Photoreceptor inner segment morphology in Best Vitelliform Macular Dystrophy. *Retina*. 2017;37(4):741–748.

23. Dooley I, Treacy M, O'Rourke M, Khaild I, Kilmartin D. Serial Spectral Domain Ocular Coherence Tomography Measurement of Outer Nuclear Layer Thickness in Rhegmatogenous Retinal Detachment Repair. *Curr Eye Res.* 2015; 40(10):1073–6.

24. Ersoz MG, Karacorlu M, Arf S, Hocaoglu M, Sayman Muslubas I. OUTER NUCLEAR LAYER THINNING IN PACHYCHOROID PIGMENT EPITHELIOPATHY. *Retina* 2018;38(5):957-961

25. Matsumoto H, Sato T, Kishi S. Outer Nuclear Layer Thickness at the Fovea Determines Visual Outcomes in Resolved Central Serous Chorioretinopathy. *American Journal of Ophthalmology*. 2009;148(1):105-110.

26. Sahel J-A, Marazova K, Audo I. Clinical characteristics and current therapies for inherited retinal degenerations. *Cold Spring Harb Perspect Med.* 2014; 5(2):a017111.

27. Staurenghi G, Sadda S, Chakravarthy U, Spaide RF, International Nomenclature for Optical Coherence Tomography (IN•OCT) Panel. Proposed lexicon for anatomic landmarks in normal posterior segment spectral-domain optical coherence tomography: the IN•OCT consensus. *Ophthalmology.* 2014; 121(8):1572–8.

28. Ctori I, Huntjens B. Repeatability of Foveal Measurements Using Spectralis Optical Coherence Tomography Segmentation Software. *PLoS ONE.* 2015; 10(6):e0129005.

29. Khan KN, Mahroo OA, Islam F, Webster AR, Moore AT, Michaelides M. FUNCTIONAL AND ANATOMICAL OUTCOMES OF CHOROIDAL NEOVASCULARIZATION COMPLICATING BEST1-RELATED RETINOPATHY. *Retina*. 2017;37(7):1360–70.

30. Qian CX, Charran D, Strong CR, Steffens TJ, Jayasundera T, Heckenlively JR. Optical Coherence Tomography Examination of the Retinal Pigment Epithelium in Best Vitelliform Macular Dystrophy. *Ophthalmology*. 2017;124(4):456–63.

31. Bakall B, Radu RA, Stanton JB, et al. Enhanced accumulation of A2E in individuals homozygous or heterozygous for mutations in BEST1 (VMD2). *Exp Eye Res.* 2007;85(1):34–43.

32. Ohkuma Y, Hayashi T, Sakai T, Watanabe A, Tsuneoka H. One-year results of reduced fluence photodynamic therapy for central serous chorioretinopathy: the outer nuclear layer thickness is associated with visual prognosis. *Graefes Arch Clin Exp Ophthalmol.* 2013;251(8):1909–17.

33. Matsumoto H, Kishi S, Otani T, Sato T. Elongation of Photoreceptor Outer Segment in Central Serous Chorioretinopathy. *American Journal of Ophthalmology.* 2008;145(1):162-168.

34. Hata M, Oishi A, Shimozono M, Mandai M, Nishida A, Kurimoto Y. Early changes in foveal thickness in eyes with central serous chorioretinopathy. *Retina.* 2013;33(2):296–301.

35. Lujan BJ, Roorda A, Croskrey JA, Dubis AM, Cooper RF, Bayabo J-K, et al. DIRECTIONAL OPTICAL COHERENCE TOMOGRAPHY PROVIDES ACCURATE OUTER NUCLEAR LAYER AND HENLE FIBER LAYER MEASUREMENTS: *Retina.* 2015;35(8):1511–20.

36. Singh R, Kuai D, Guziewicz KE, et al. Pharmacological Modulation of Photoreceptor Outer Segment Degradation in a Human iPS Cell Model of Inherited Macular Degeneration. *Molecular Therapy.* 2015;23(11):1700–11.

The authors have no proprietary interest in the materials used in this study.

Figure 1. Short wavelength fundus autofluorescent pictures of the posterior pole (left column) for the five clinical stages in Best vitelliform macular dystrophy and their corresponding optical coherence tomography scans (right column). (A) Previtelliform stage. A slight foveal thickening of the interdigitation zone is seen (white arrow). The outer nuclear layer (ONL) thickness and visual acuity were both normal. (B) Vitelliform stage. Onset of vitelliform material (VM) accumulation and separation between the photoreceptor outer segments (PROS) and the retinal pigment epithelium due to the accumulation of VM. (C) Pseudohypopyon stage. The apical projection of the PROS is clearly identifiable within the subretinal detachment, although we can observe the beginning of disintegration in the perifoveolar region (white arrow). The ONL is still conserved, as well as visual acuity (20/25). 4. Vitelliruptive stage (Same eye as in picture C, 29 months later). PROS length (yellow arrows) and ONL thickness (red arrows) are severely reduced. Visual acuity is decreased (20/50). 5. Atrophic stage. The subretinal fluid has completely disappeared. There is significant retinal atrophy with almost no foveolar ONL. Visual acuity is collapsed (20/400).

Figure 2. Algorithm details of spectral domain optical coherence tomographic (SD-OCT) measurements using the Heidelberg analysis software (Heidelberg Engineering, Germany). (A) Infrared photograph of the right posterior pole of a 33-year old patient with a pseudohypopion lesion. Horizontal line shows the position of the sectional SD-OCT automatically located across the fovea. The central macular thickness was determined automatically within a 1-mm diameter circle centered on the fovea. (B) Corresponding horizontal SD-OCT scan. The foveal outer nuclear layer (ONL) thickness was measured manually through the center of fovea (white segment). The value of the photoreceptor outer segment length (PROSL) above the subretinal detachment was the mean of three regular measurements around the center of the fovea (500 µm on both sides).

Figure 3. Correlation analysis. Regression plots showing the correlations between visual acuity (VA), age (A), foveal outer nuclear layer (ONL) thickness (B), central macular retinal thickness (CMT) (C) and photoreceptor outer segment (PROS) length within the subretinal detachment (D).

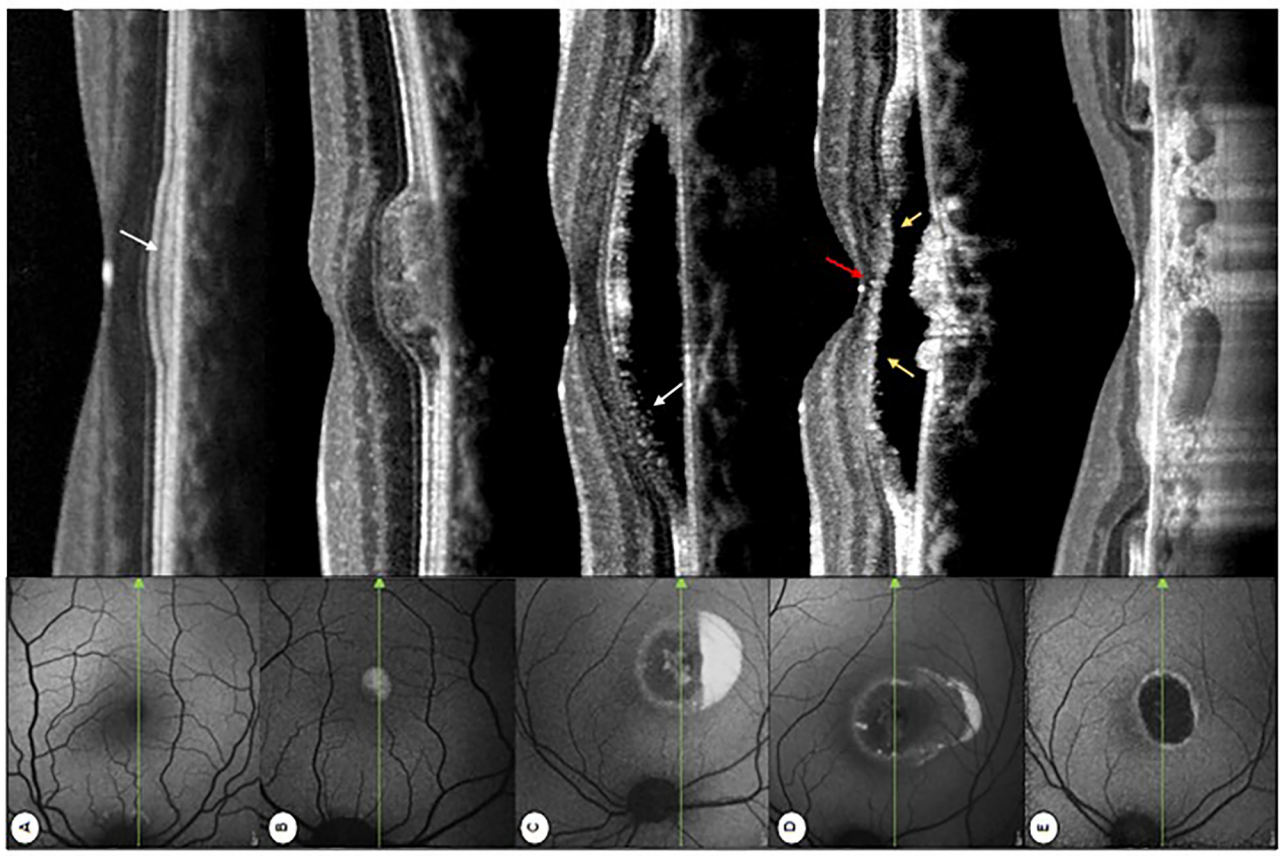
A
B
C
D
E

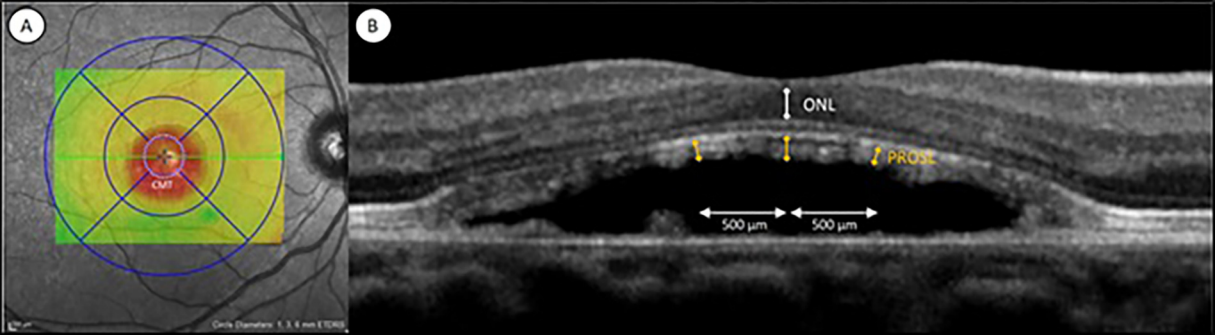
A
CMT
B
ONL
PROS
500 µm
500 µm

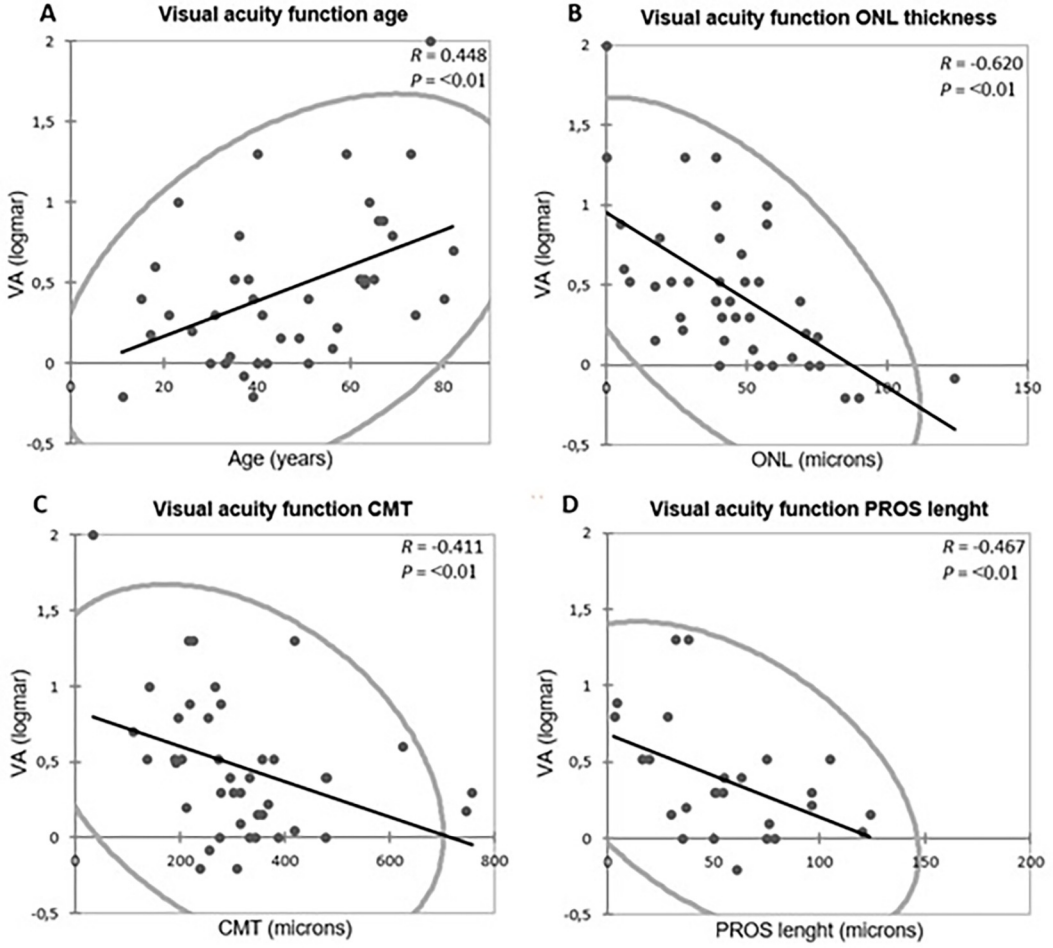
A
Visual acuity function age
R = 0.448
P = <0.01
VA (logmar)
Age (years)
B
Visual acuity function ONL thickness
R = -0.620
P = <0.01
VA (logmar)
ONL (microns)
C
Visual acuity function CMT
R = -0.411
P = <0.01
VA (logmar)
CMT (microns)
D
Visual acuity function PROS lenght
R = -0.467
P = <0.01
VA (logmar)
PROS lenght (microns)

Table 1. Demographic and ophthalmic characteristics

	Stage 1 (n=2)	Stage 2 (n=10)	Stage 3 (n=7)	Stage 4 (n=19)	Stage 5 (n=4)	All (n=42)	Controls (n=42)
Demographic characteristics							
Age, year	38	38.1	39.0	52.0	63.3	43.5	44.4
Male, %	50	41	39	59	66	43	42
Ophthalmic characteristics							
BCVA median, logMAR	-0.14	0.10	0.19	0.52	0.90	0.40	0
BCVA median, Snellen equivalent	20/16	20/25	20/32	20/63	20/160	20/50	20/20

Table 2. OCT characteristics

	Stage 1 (n=2)	Stage 2 (n=10)	Stage 3 (n=7)	Stage 4 (n=19)	Stage 5 (n=4)	All (n=42)	Controls (n=42)	*P* value(1)
CST, µm [range]	247[19]	416[724]	331[124]	273[307]	168[170]	298[724]	281[87]	0.38
ONL thickness, µm	105[21]	65[24]	52[76]	39[57]	21[55]	42[124]	96[51]	< 0,0001
Subretinal fluid, %	0	60	100	90	50	76	0	NA
Vitelliform material, %	0	100	86	79	50	79	0	NA
Outer retinal defects, %								
External Limiting Membrane	0	50	67	84	100	62	0	NA
Ellipsoid zone	0	80	86	95	100	83	0	NA
PROSL within SRD, µm	NA	66[49]	63[90]	50[82]	28[NA]	53[121]	NA	NA

NA : Not appropriate analysis

(1) Mann-Whithney test between all the BVMD patients and the controls.

Table 3. Spearman coefficient correlation matrix for BCVA and OCT parameters.

		BCVA logMAR
Central Macular thickness	*R*	-0.411
	P	< 0.01
Foveal Outer Nuclear Layer thickness	*R*	-0.620
	P	< 0.01
Photoreceptor Outer Segments length within the SRD	*R*	-0.467
	P	<0.01
Age	*R*	0.448
	P	<0.01
Stage	*R*	0.710
	P	< 0.01

Table 4. Ophthalmic and OCT characteristics of eyes with available follow-up

	Eyes (n=21)	*P value*[(1)]
Median follow up, month (range)	49[72]	
BCVA variation, logMAR	-0.19	0.003
Stage modification, %	33	NA
OCT modification		
CST, µm	-40	0.340
PROSL within SRD, µm	-4.0	0.920
ONL thickness, µm	-9.2	<0.001

NA : Not appropriate analysis
(1) Wilcoxon test between the first and last measurements